DOI: 10.30511/jmms.2026.2083299.1037 - ISSN: 3060-8384 - Vol 2(2), 2026

MECHANICS OF SMART STRUCTURES
Available Online at: http://jmss.qut.ac.ir/

QOM UNIVERSITY OF TECHNOLOGY

Adaptive Control of a Lower-Limb Rehabilitation Robot Using High-Gain and Disturbance Observers Under Sensor Noise and External Disturbances

ARTICLE INFO

Article Type
Original Research

Authors
Atefe Behboodi[1], Ali Keymasi-Khalaji[2]

[1] M.Sc. Student, Faculty of Engineering, Department of Mechanical Engineering, Kharazmi University, Tehran, Iran, behboodiatefe@gmail.com
[2] M.Sc. Student, Faculty of Engineering, Department of Mechanical Engineering, Kharazmi University, Tehran, Iran, behboodiatefe@gmail.com

**** Correspondence***
Address: Department of mechanical engineering, Faculty of engineering , Iran.
keymasi@khu.ac.ir

Article History
Received: January 30 , 2026
Accepted: July 22 , 2026
ePublished: August 2 , 2026

ABSTRACT

Rehabilitation robots are advanced systems designed to assist injured individuals by providing targeted support and facilitating therapeutic exercises, thereby helping to improve physical functions following injuries or medical interventions. This study focuses on the modeling and controller design of a rehabilitation robot. In the modeling section, the robot is considered as a planar three-degree-of-freedom serial robot to enable the actuation of the hip, knee, and ankle joints. The dynamic model of the robot is derived using the Euler–Lagrange method. Furthermore, with the increasing emphasis on robot-assisted rehabilitation, the need for adaptive control systems to tailor treatment to the individual needs of patients has become critically important. Therefore, due to the variability and uncertainty of the robot parameters, an adaptive controller is employed. In addition, considering the presence of noise in sensor data and disturbances arising from the interaction between the robot and the patient, a High-Gain Observer is used to estimate the system state variables, and a disturbance observer is utilized to estimate and compensate for disturbance effects. The simulation results show that, in the nominal case without sensor noise and external disturbances, the mean tracking errors of the hip, knee, and ankle joints are 0.0025, 0.0024, and 0.0039 rad, respectively. When sensor noise and external disturbances are applied without observers, the adaptive controller alone becomes unstable. By incorporating the High-Gain Observer and nonlinear disturbance observer, the mean tracking errors are limited to

0.004, 0.017, and 0.025 rad for the three joints, respectively, remaining below 0.05 rad.

Keywords: Lower-limb rehabilitation robot, adaptive controller, High-Gain Observer, nonlinear disturbance observer .

1-1 Introduction

With the advancement of robotics, robots can be found in a wide range of applications. One of the important applications of robots is in the medical field, particularly in rehabilitation. Rehabilitation robots are designed to assist individuals with various motor impairments resulting from injuries, surgeries, or neurological conditions. Analysis of data from the Global Burden of Disease (GBD) study in 2019 showed that the number of strokes increased by 70% between 1990 and 2019 [1]. Especially with the growth of the elderly population and people with disabilities, and the increasing prevalence of conditions affecting mobility, rehabilitation care has become increasingly important [2-4].

Research has shown that patients can regain a significant portion of their functional abilities through occupational therapy. For this reason, physiotherapists help patients achieve this goal more rapidly by designing appropriate exercises. However, performing these exercises without assistance is difficult for many patients. In such circumstances, rehabilitation robots assist patients and have been developed as dynamic tools to support, enhance, and accelerate the rehabilitation process.

The use of robots requires appropriate control systems, and extensive research has been conducted in this area. Du et al. proposed an advanced adaptive control method for a lower-limb rehabilitation robot using brain signals [5]. The results of their experiments showed that the designed system was able to effectively reduce trajectory tracking errors. Tu et al. designed a control system for a lower-limb rehabilitation robot based on an adaptive sliding mode control method with variable admittance [6]. They demonstrated that their proposed controller achieved higher accuracy compared to conventional sliding mode controllers. Gao et al. designed an admittance-based control system using a particle swarm optimization metaheuristic algorithm [7]. Their results indicated that this algorithm enhanced human–robot interaction, increased flexibility, and enabled improved walking performance.

In all three of the aforementioned studies, the robots were considered for hip and knee rehabilitation. In other words, these studies focused on the design of controllers for two-degree-of-freedom robots. Moreover, the effects of noise on system performance were not investigated in these studies.

The present study focuses on the modeling and control of a three-degree-of-freedom lower-limb rehabilitation robot. To this end, Section 2 of the paper addresses the modeling of the dynamic behavior of the three-degree-of-freedom robot. Due to variations in patient dimensions and conditions, patient–robot interaction, and other external factors, the robot under consideration exhibits significant uncertainty in its physical parameters. Therefore, designing a controller that ensures proper robot performance in the presence of these uncertainties is essential.

In Section 3, an adaptive controller is designed to address this challenge. Considering the presence of noise in position sensor data, a High-Gain Observer (HGO) is proposed to estimate the system state variables. Finally, to compensate for disturbances acting on the system (or the effects of patient–robot interaction), a nonlinear disturbance observer is employed. The designed control system is simulated using MATLAB software, and the results are analyzed and discussed in the final section.

1-2 Dynamic Modeling of the Rehabilitation Robot

The robot under consideration is modeled as a planar three-degree-of-freedom robot. The dynamic equations governing the dynamics of serial robots can be expressed as

$$M(q)\ddot{q} + C(q,\dot{q})\dot{q} + G(q) = \tau \tag{1}$$

where $M \in R^{n\times n}$ is the robot inertia matrix, $C \in R^{n\times n}$ is the Coriolis matrix, and $G \in R^{n}$ is the gravity effects vector. Figure 1 illustrates a schematic of a rehabilitation robot modeled as a planar three-degree-of-freedom serial robot.

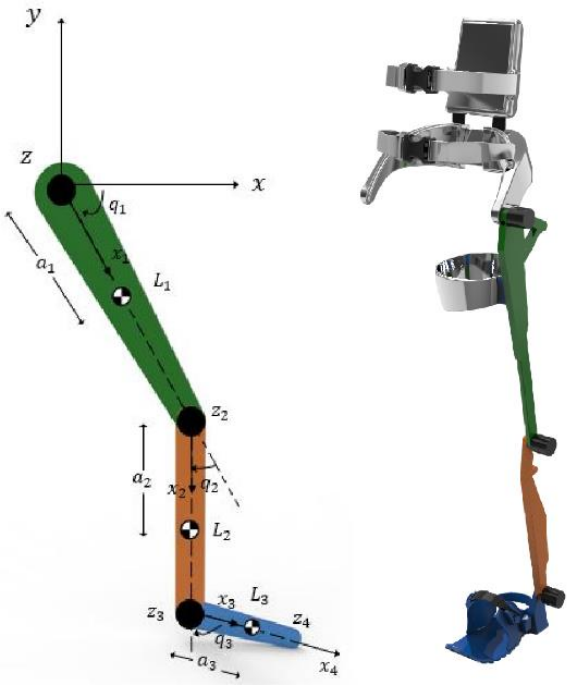


Figure 1: Schematic of the robot.

For a planar three-degree-of-freedom robot, the elements of the above matrices and vectors are given as

$$
\begin{aligned}
&M(1,1) = \theta(1) + \theta(2) + \theta(3) + 2\theta(4)c_2 + 2\theta(5)c_{23} + 2\theta(6)c_3 \\
&M(2,2) = \theta(2) + \theta(3) + 2\theta(6)c_3 \\
&M(3,3) = \theta(3) \\
&M(2,1) = M(1,2) = \theta(2) + \theta(3) + \theta(4)c_2 + \theta(5)c_{23} + 2\theta(6)c_3 \\
&M(3,1) = M(1,3) = \theta(3) + \theta(5)c_{23} + \theta(6)c_3 \\
&M(3,2) = M(2,3) = \theta(3) + \theta(6)c_3
\end{aligned}
\tag{2}
$$

$$
\begin{aligned}
&C(1,1) = -\theta(4)\dot{q}_2 s_2 - \theta(5)(\dot{q}_2 + \dot{q}_3)s_{23} - \theta(6)\dot{q}_3 s_3 \\
&C(2,2) = -\theta(6)\dot{q}_3 s_3 \\
&C(3,3) = 0 \\
&C(2,1) = \theta(4)\dot{q}_1 s_2 + \theta(5)\dot{q}_1 s_{23} - \theta(6)\dot{q}_3 s_3 \\
&C(1,2) = -\theta(4)(\dot{q}_1 + \dot{q}_2)s_2 - \theta(5)(\dot{q}_1 + \dot{q}_2 + \dot{q}_3)s_{23} - \theta(6)\dot{q}_3 s_3 \\
&C(3,1) = \theta(6)(\dot{q}_1 + \dot{q}_2)s_3 + \theta(5)\dot{q}_1 s_{23} \\
&C(1,3) = -(\theta(6)s_3 + \theta(5)s_{23})(\dot{q}_1 + \dot{q}_2 + \dot{q}_3) \\
&C(3,2) = \theta(6)(\dot{q}_1 + \dot{q}_2)s_3 \\
&C(2,3) = -\theta(6)s_3(\dot{q}_1 + \dot{q}_2 + \dot{q}_3)
\end{aligned}
\tag{3}
$$

$$
\begin{aligned}
G(1) &= \theta(7)c_1 + \theta(8)c_{12} + \theta(9)c_{123} \\
G(2) &= \theta(8)c_{12} + \theta(9)c_{123} \\
G(3) &= \theta(9)c_{123}
\end{aligned} \tag{4}
$$

In the above equations, the values of $\theta(i)$ are given in Eq. (7), where m_i ،I_i ،l_i and a_i represent the mass, moment of inertia, link length, and the location of the link center of mass, respectively. In addition, $s_{ij} = \sin(q_i + q_j)$ and $c_{ij} = \cos(q_i + q_j)$. It can be shown that the dynamics of a serial robot are linearizable with respect to its physical parameters. In other words:

$$M(q)\ddot{q} + C(q,\dot{q}) + G(q) = Y(q,\dot{q},\ddot{q})\theta \tag{5}$$

where the matrix $Y \in R^{n\times p}$ is called the regressor matrix, and $\theta \in R^p$ is the vector of the robot's physical parameters. The elements of the regressor matrix and the parameter vector are given by

$$
\begin{aligned}
Y(1,1) &= \ddot{q}_1 \\
Y(1,2) &= Y(2,2) = \ddot{q}_1 + \ddot{q}_2 \\
Y(1,3) &= Y(2,3) = Y(3,3) = \ddot{q}_1 + \ddot{q}_2 + \ddot{q}_3 \\
Y(1,4) &= c_2(2\ddot{q}_1 + \ddot{q}_2) - s_2(2\dot{q}_1\dot{q}_2 + \dot{q}_2^2) \\
Y(1,5) &= c_{23}(2\ddot{q}_1 + \ddot{q}_2 + \ddot{q}_3) - s_{23}(2\dot{q}_1\dot{q}_2 + 2\dot{q}_1\dot{q}_3 + 2\dot{q}_2\dot{q}_3 + \dot{q}_2^2 + \dot{q}_3^2) \\
Y(1,6) &= c_3(2\ddot{q}_1 + 2\ddot{q}_2 + \ddot{q}_3) - s_3(2\dot{q}_1\dot{q}_3 + 2\dot{q}_2\dot{q}_3 + \dot{q}_3^2) \\
Y(2,4) &= c_2\ddot{q}_1 + s_2\dot{q}_1^2 \\
Y(2,5) &= Y(3,5) = c_{23}\ddot{q}_1 + s_{23}\dot{q}_1^2 \\
Y(2,6) &= c_3(2\ddot{q}_1 + 2\ddot{q}_2 + \ddot{q}_3) - s_3(2\dot{q}_1\dot{q}_3 + 2\dot{q}_2\dot{q}_3 + \dot{q}_3^2) \\
Y(3,6) &= c_3(\ddot{q}_1 + \ddot{q}_2) + s_3(\dot{q}_1 + \dot{q}_2)^2 \\
Y(1,7) &= c_1 \\
Y(1,8) &= Y(2,8) = c_{12} \\
Y(1,9) &= Y(2,9) = Y(3,9) = c_{123} \\
Y(2,1) &= Y(2,7) = Y(3,1) = Y(3,2) = Y(3,4) = Y(3,7) = Y(3,8) = 0
\end{aligned} \tag{6}
$$

$$
\begin{aligned}
\theta(1) &= m_1a_1^2 + m_2l_1^2 + m_3l_1^2 + I_1 \\
\theta(2) &= m_2a_2^2 + m_3l_2^2 + I_2 \\
\theta(3) &= m_3a_3^2 + I_3 \\
\theta(4) &= m_2l_1a_2 + m_3l_1l_2 \\
\theta(5) &= m_3a_3l_1 \\
\theta(6) &= m_3a_3l_2 \\
\theta(7) &= g(m_1a_1 + m_2l_1 + m_3l_1) \\
\theta(8) &= g(m_2a_2 + m_3l_2) \\
\theta(9) &= gm_3a_3
\end{aligned} \tag{7}
$$

1-3 Design of a Passivity-Based Adaptive Controller

The structure of rehabilitation robots is generally designed to be adjustable in size so that it can be used for different patients. As a result, the physical parameters of the robot are variable. This variability leads to uncertainty in the physical parameters and obliges the designer to employ an adaptive controller. Accordingly, this section is devoted to the design of an adaptive controller for the robot.

If the desired input for the robot is considered as q_d, the tracking error is defined as $e = q - q_d$ In addition, the variables v and s are defined according to Eqs. (8) and (9), respectively

$$v = \dot{q}_d - \Lambda_0(q - q_d) \tag{8}$$
$$s = \dot{q} - v = \dot{e} + \Lambda_0 e \tag{9}$$

where $\Lambda_0 \in R^{n\times n}$ is a constant matrix with positive and real eigenvalues. Therefore:

$$\begin{aligned} &M(q)\dot{s} + C(q,\dot{q})s \\ &= \tau - M(q)\dot{v} + C(q,\dot{q})v - G(q) \\ &\triangleq \tau - Y(q, q_d, \dot{q}, \dot{q}_d, \ddot{q}_d)\theta^* \end{aligned} \tag{10}$$

In the above equation, θ^* has constant values. The control law is defined as

$$\tau = Y(q, q_d, \dot{q}, \dot{q}_d, \ddot{q}_d)\theta - K_D s \tag{11}$$
$$\dot{\theta} = -\Gamma^{-1} Y^T(q, q_d, \dot{q}, \dot{q}_d, \ddot{q}_d)s \tag{12}$$

where $0 < K_D = K_D^T \in R^{n\times n}$ and $0 < \Gamma = \Gamma^T \in R^{p\times p}$ It can be shown that, by using the defined control law, the closed-loop system possesses global stability. For this purpose, the Lyapunov candidate function is chosen as given in Eq. (13).

$$V(s, \tilde{\theta}) = \frac{1}{2}\left(s^T M s + \tilde{\theta}^T \Gamma \tilde{\theta}\right) \tag{13}$$

where $\tilde{\theta} = \theta - \theta^*$. By differentiating the Lyapunov candidate function, we obtain:

1 . (14)

$$= -s^T K_D s + \tilde{\theta}^T \left(Y^T s + \Gamma \dot{\tilde{\theta}} \right)$$
$$= -s^T K_D s < 0$$

It should be noted that, first, $\dot{\tilde{\theta}} = \dot{\theta}$, and second, $\dot{M} - 2C$ is a skew-symmetric matrix; therefore, $s^T(\dot{M} - 2C)s = 0$.

1-4 High-Gain Observer (HGO) Design

Since the sensors used in robots are generally intended to measure joint angles, the angular velocities required in the control system must be obtained from the position signal. However, due to the presence of noise in the position measurement, direct differentiation to compute angular velocity leads to system instability. Therefore, in this section, for a system with a state-space representation in the form of Eq. **Error! Reference source not found.**, a high-gain observer is proposed to estimate the state variables according to Eq. (16) [8].

$$\begin{aligned} \dot{x} &= f(x) + g(x)u \\ y &= h(x) \end{aligned} \tag{15}$$

$$\dot{\hat{x}} = f(\hat{x}) + g(\hat{x})u + H[y - h(\hat{x})] \tag{16}$$

In Eq. (17), $\hat{x}$ denotes the estimated value of the system state variables, and H is the observer gain.

1-5 Disturbance Observer Design

Due to the interaction between the robot and the patient, an additional torque arises on the joints beyond the torque applied by the robot actuators ($u = \tau + d$). This torque can be reasonably approximated as a constant disturbance (d) In this section, in order to estimate and compensate for this disturbance, the observer proposed in [9, 10] is employed (Eq. (17)).

$$\begin{aligned} \dot{z} &= -L_d g(x) z - L_d \left[f(x) + g(x)\left(\tau + p(x)\right) \right] \\ \hat{d} &= z + p(x) \end{aligned} \tag{17}$$

In the above equation, $\hat{d}$ is the estimated disturbance, z is the internal state variable of the observer, $p(x)$ is the auxiliary vector, and L_d is the observer gain matrix. Moreover, Eqs. (18) and (19) hold for the auxiliary vector and the observer gain, respectively.

$$L_d(x) \coloneqq \alpha_d g^{\dagger}(x), \quad g^{\dagger}(x) = \left(g^T(x)g(x)\right)^{-1} g^T(x) \tag{18}$$

$$L_d(x) = \frac{\partial}{\partial x} p(x) \tag{19}$$

If $e_d = \hat{d} - d$, then we have:

$$\begin{aligned} \dot{e}_d &= \dot{\hat{d}} - \dot{d} \\ &= \dot{z} + \frac{\partial p(x)}{\partial x}\dot{x} \\ &= -L_d g(x) z - L_d\left[f(x) + g(x)\left(\tau + p(x)\right)\right] + L_d[f(x) + g(x)(\tau + d)] \\ &= -L_d g(x)\hat{d} + L_d g(x) d \\ &= -L_d g(x) e_d \end{aligned} \tag{20}$$

From Eq. (20), it can be inferred that the proposed observer is able to estimate a constant disturbance, provided that for the selected L_d Eq. (20) is asymptotically stable. For the robot under consideration, if the state variables are defined as $x = [q, \dot{q}]^T$, the matrices $f(x)$ and $g(x)$ are obtained accordingly and are given in the form of Eqs. (21) and (22).

$$f(x) = \begin{bmatrix} 0_{3\times 1} \\ -M^{-1}(q)\left(C(q,\dot{q})\dot{q} + G(q)\right) \end{bmatrix} \tag{21}$$

$$g(x) = \begin{bmatrix} 0_{3\times 3} \\ M^{-1}(q) \end{bmatrix} \tag{22}$$

1-6 Results

In this section, the simulation and evaluation of the designed controller are addressed. For this purpose, the robot parameters are considered according to the values given in Table 1.

Table 1: Physical Specifications of the Rehabilitation Robot

Unit	Value	Parameter
kg	0.967	m_1
	0.605	m_2
	0.721	m_3
$kg.m^2$	1	I_1
	1	I_2
	0.530	I_3
m	0.520	l_1

	0.405	l_2
	0.213	l_3
	0.260	a_1
	0.202	a_2
	0.106	a_3

The reference input and the disturbance are considered according to Eqs. (23) and (24), respectively. In addition, the sensor noise was modeled using band-limited Gaussian white noise with zero mean, a sampling time of 0.01 s, and a standard deviation of 0.01 rad for each joint position measurement. This value corresponds to approximately $0.57°$, which is consistent with practical joint-angle measurement uncertainty in rehabilitation systems when sensor resolution, quantization, mounting misalignment, calibration error, and electrical noise are considered.

$$q_d = \begin{bmatrix} \frac{\pi}{12}(1-\cos(\pi t)) \\ \frac{\pi}{4}(\cos(\pi t)-1) \\ \frac{\pi}{2}+\frac{\pi}{10}\sin(\pi t) \end{bmatrix} \tag{23}$$

$$d = [0.5, 0.5, -0.25]^T \tag{24}$$

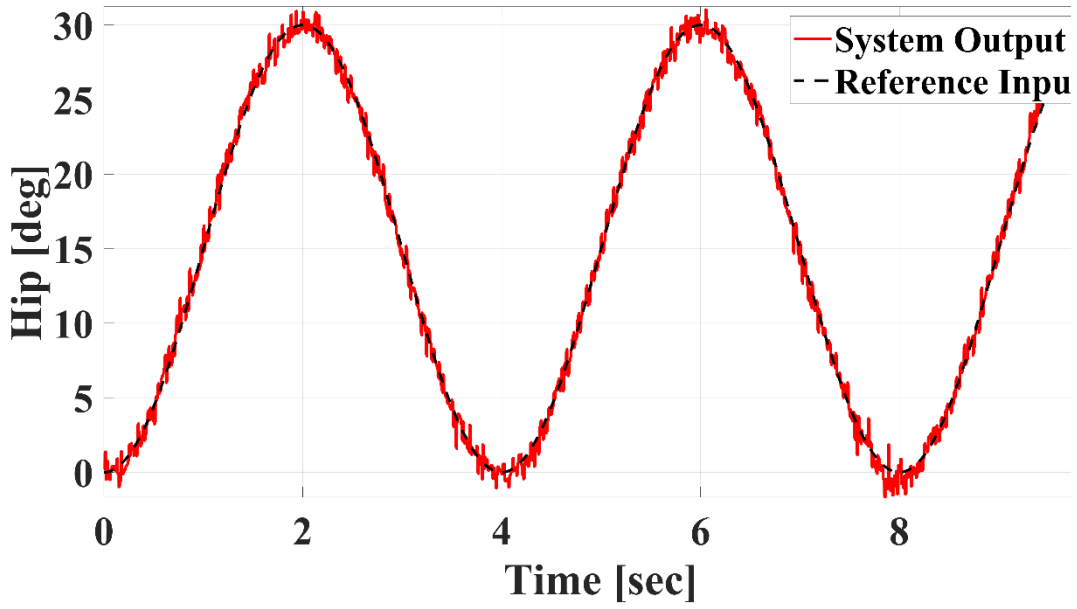
The disturbance represents an external joint torque caused by patient-robot interaction and unmodeled external effects. Therefore, its unit is N.m.

The controller and observer gains were selected through a step-by-step tuning procedure. First, $\Lambda_0$was chosen based on the desired convergence rate of the filtered tracking error $s = \dot{e} + \Lambda_0 e$. A larger value of Λ_0 improves tracking speed but may increase the required control torque. In this study, $\Lambda_0 = 10I^3$ was selected as a compromise between tracking performance and control smoothness. Next, K_D was tuned to damp the filtered error dynamics. The value $K_D = 7I^3$ provided sufficient damping without generating excessive control effort. The adaptation matrix was set to $\Gamma = 0.1I^9$, which resulted in stable parameter adaptation without high-frequency oscillations. The high-gain observer was tuned using a second-order pole-placement approach. By selecting an observer bandwidth of $\omega_o = 10\ \text{rad/s}$, the observer gains become $h_1 = 2\omega_o = 20$ and $h_2 = \omega_o^2 = 100$, leading to $H = \text{diag}([20I^3, 100I^3])$. This choice provides a balance between fast state estimation and noise amplification.

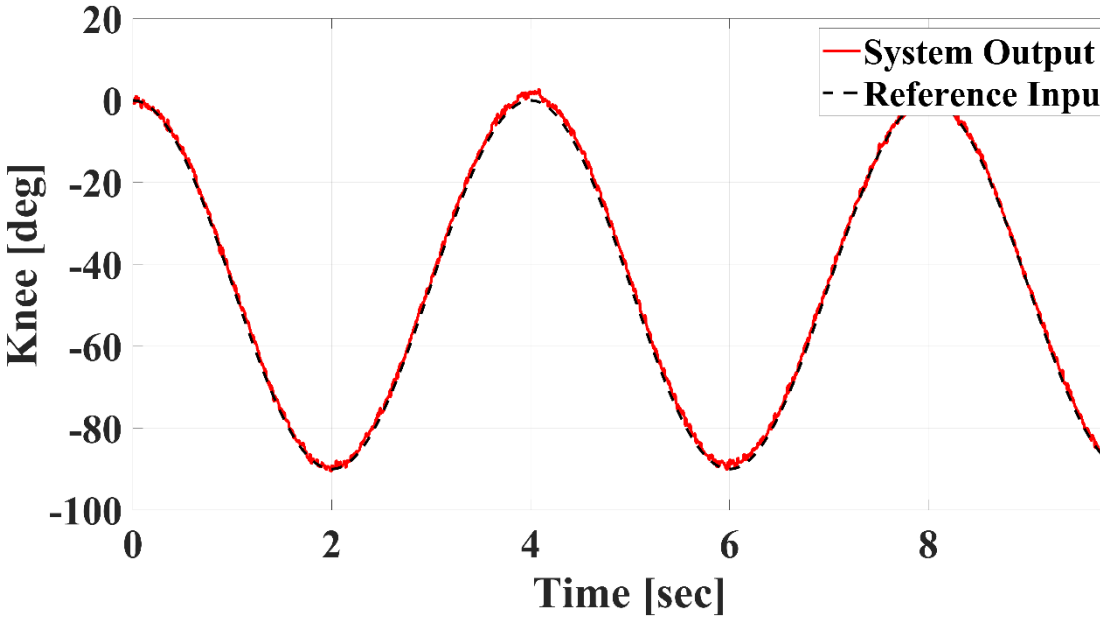
The disturbance observer contains one main tuning coefficient, denoted by α_d. The auxiliary function was selected as $p(x) = \alpha_d \dot{q}$. Therefore, $L_d(x) = \partial p(x)/\partial x = [0_{3\times3}\,;\alpha_d I^3]$. Since the input matrix of the robot is $g(x) = [0_{3\times3}\,;\ M^{-1}(q)]^T$, the disturbance estimation error dynamics

are obtained as $\dot{e}_d = -\alpha_d M^{-1}(q) e_d$. Because $M(q)$ is positive definite, $M^{-1}(q)$ is also positive definite; therefore, the disturbance estimation error converges asymptotically for any $\alpha_d > 0$. Increasing α_d accelerates disturbance estimation but may increase noise sensitivity. In this study, $\alpha_d = 20$ was selected as a compromise between fast disturbance estimation and robustness against sensor noise. Therefore, $L(x) = 20I^3 M^{-1}(q)$ and $p(x) = 20I^3 x_2$ where $I^i \in R^{i \times i}$ denotes the identity matrix.

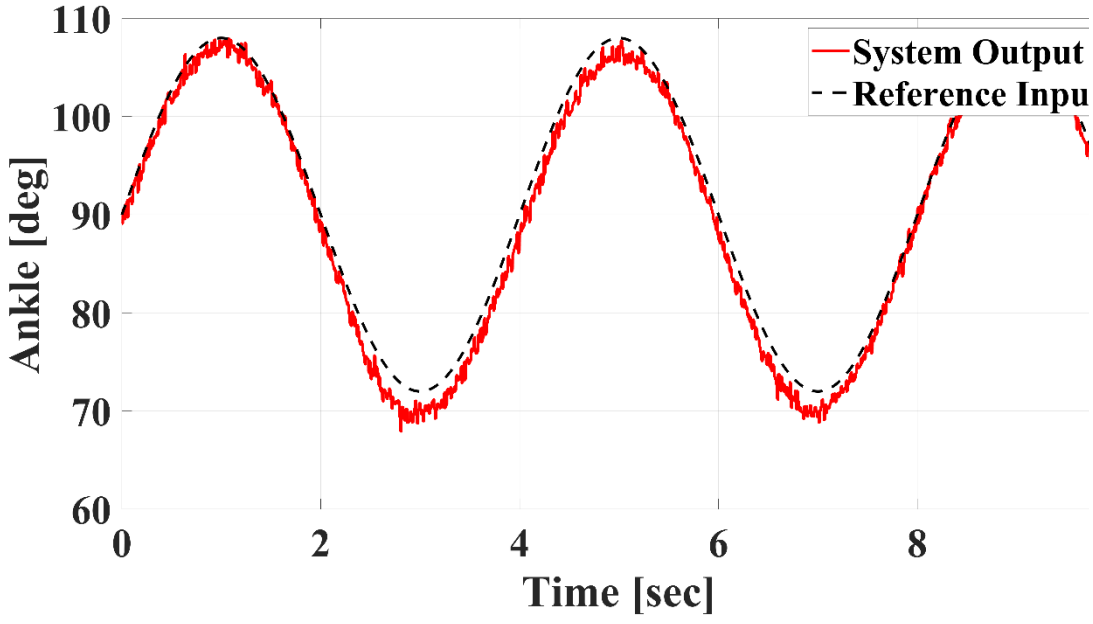
The simulation results of the designed system are presented in Figures 2 to 5. Figure 2 shows the reference input and the outputs of the position sensors mounted on the joints. Figure 3 illustrates the controller output (control effort) for all three joints. In order to compare the derivative of the position sensor signal with the angular velocity estimated using the high-gain observer, the corresponding plots for the hip joint are provided in Figure 4. Finally, Figure 5 depicts the disturbance applied to the system and its estimated value.



(a)


System Output
Reference Inpu
Knee [deg]
20
0
-20
-40
-60
-80
-100
0
2
4
6
8
Time [sec]

(b)


System Output
Reference Inpu
Ankle [deg]
110
100
90
80
70
60
0
2
4
6
8
Time [sec]

(c)

Figure 2: Reference input and system output for the joints:

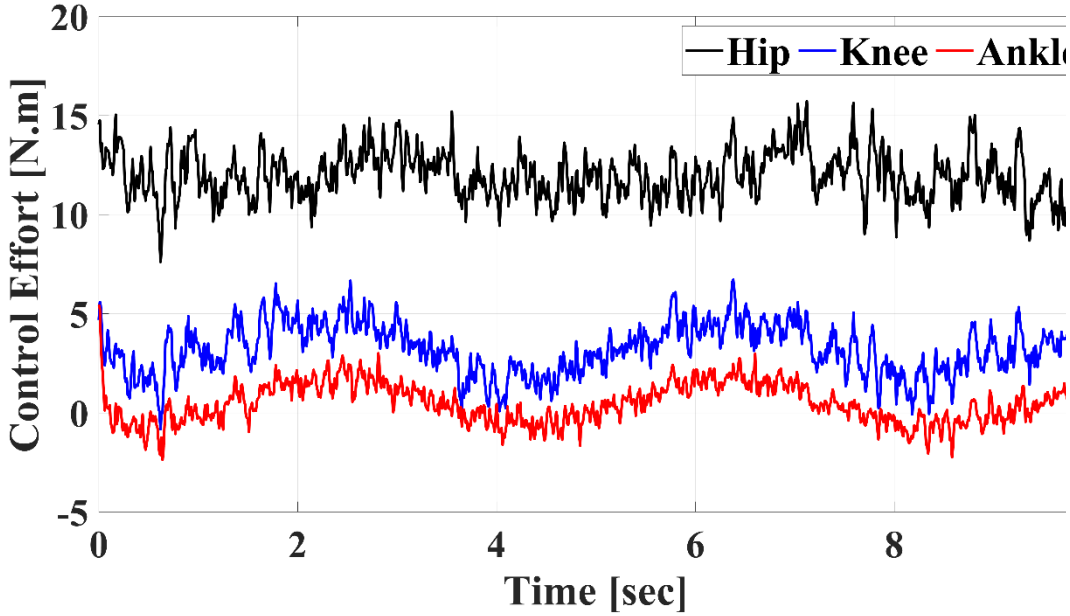


Figure 3: Control effort for all three robot joints.

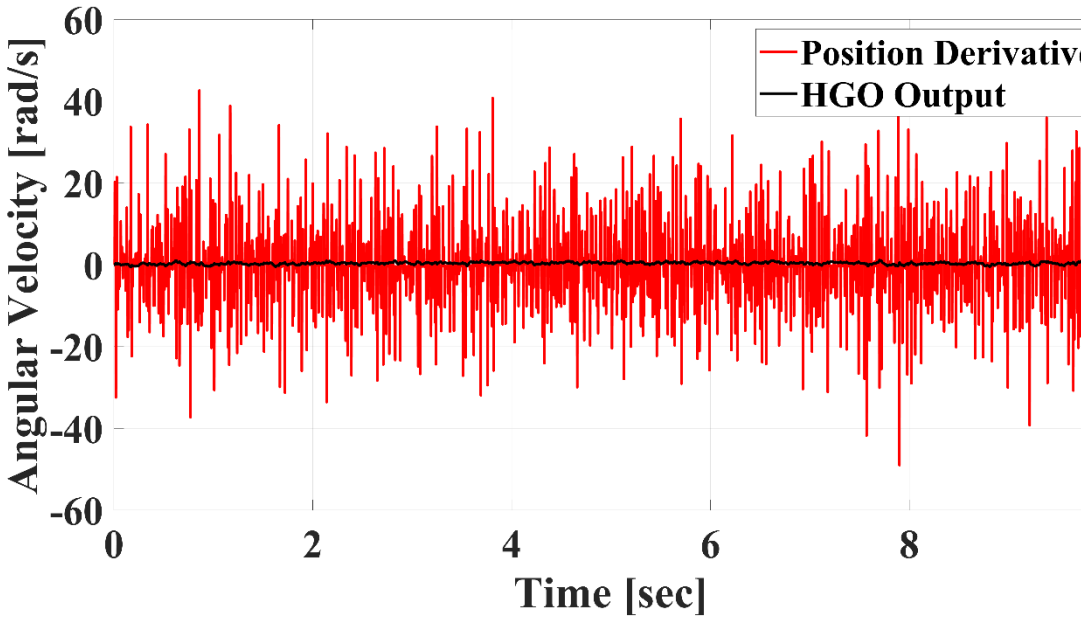


Figure 4: Comparison between the derivative of the hip joint position signal and the value estimated using the high-gain observer.

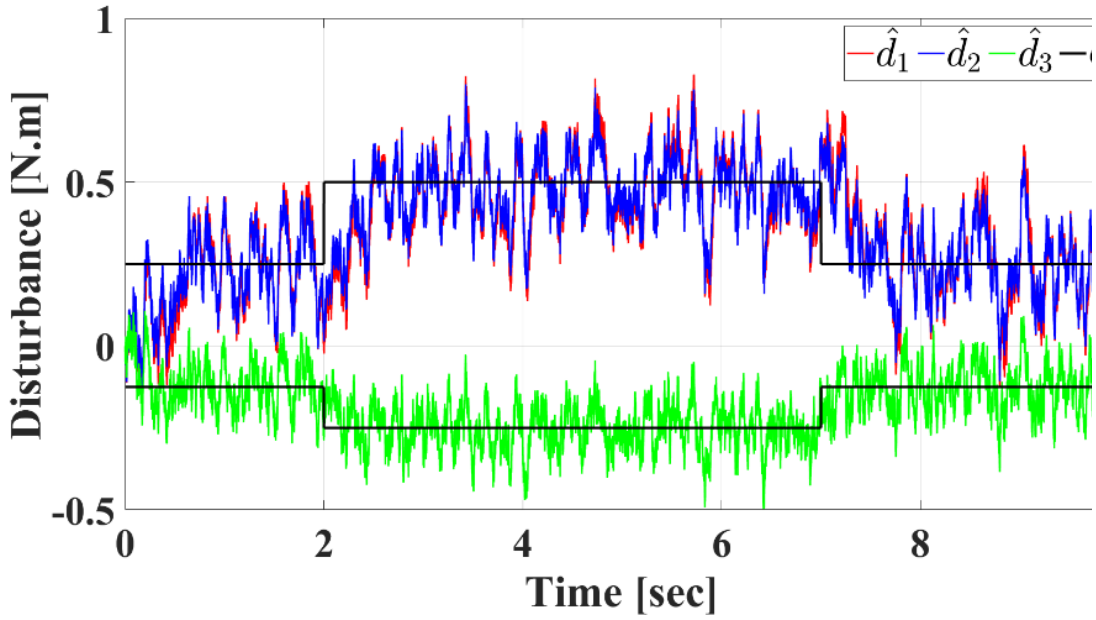


Figure 5: The disturbance applied to the system and the values identified using the disturbance observer.

In order to evaluate the performance of the designed control system, the mean tracking error is defined according to the following equation.

$$E_i = \frac{\int_0^{t_f} e_i(t)dt}{t_f}, \quad i = 1,2,3 \tag{25}$$

where t_f denotes the simulation time which is 10 seconds for all simulations. Accordingly, the simulation results obtained under different conditions are presented in Table 2.

Table 2: Control system error under different conditions.

E_3	E_2	E_1	Conditions
0.0039	0.0024	0.0025	Without noise and disturbance – without observer
Unstable			With noise and disturbance – without observer

Reviewer 1.7

0.0245	0.0167	0.0033	With noise and disturbance – with observer

It is observed that when noise and disturbances are added to the system, the adaptive controller alone is not able to maintain system stability. However, by incorporating observers, the tracking error is significantly reduced. Moreover, in the presence of noise and disturbances and with the use of observers, the maximum errors of the joints are respectively equal to 0.01 rad, 0.03 rad, and 0.05 rad. It should be noted that, the errors of Joints 2 and 3 are larger than Joint 1 because these distal joints are more strongly affected by dynamic coupling, gravity terms, and propagation of estimation errors through the serial-chain dynamics.

For comparison, a sliding mode controller, defined in Eqs. (26) and (27), is designed and simulated.

$$\dot{S} = -k|S|^{p}\mathrm{sgn}(S) \tag{26}$$

$$\tau = M\left(\dot{S} + a\dot{e}_q + \ddot{q}_d\right) + C(q,\dot{q})\dot{q} + G(q) \tag{27}$$

Where S is the sliding surface; $\mathrm{sgn}(\cdot)$ is the sign function; $k = 8$, $a = 6$ and $p = 0.15$ are controller parameters. Results show that the mean tracking error for this controller without applying any disturbance and sensor noise are $E_1 = 0.0024$, $E_2 = 0.0036$, and $E_3 = 0.0069$ which are higher than error of the proposed adaptive controller in the same condition. Moreover, the sign function causes chattering in the control effort signal that may damage the actuators.

1-7 Conclusion

This paper presented the dynamic modeling and adaptive control of a three-degree-of-freedom lower-limb rehabilitation robot. The robot was modeled as a planar serial mechanism representing the hip, knee, and ankle joints, and a passivity-based adaptive controller was designed to address uncertainty in the physical parameters. To account for practical sensing and interaction effects, a HGO was used to estimate the state variables from noisy position measurements, and a nonlinear disturbance observer was employed to estimate and compensate external joint torques caused by patient-robot interaction. In the nominal case without noise and disturbance, the mean tracking errors of the three joints were 0.0025, 0.0024, and 0.0039 rad, respectively. When noise and disturbances were added without observers, the adaptive controller alone became unstable. After adding the HGO and disturbance observers, the mean tracking errors were reduced to 0.0033, 0.0167, and 0.0245 rad, respectively, demonstrating that the proposed observer-based adaptive structure can maintain stable tracking with errors below 0.05 rad. Future work will focus on experimental implementation on a physical rehabilitation platform, validation using realistic

sensor data and patient-interaction forces, and extension of the control framework to a six-degree-of-freedom lower-limb rehabilitation robot.

1-8 References

[1] C. W. Tsao, A. W. Aday, Z. I. Almarzooq, C. A. Anderson, P. Arora, C. L. Avery, *et al.*, "Heart disease and stroke statistics—2023 update: a report from the American Heart Association," *Circulation*, vol. 147, pp. e93-e621, 2023.

[2] I. G. Aprile et al., "Identifying needs in adult rehabilitation to support the clinical implementation of robotics and allied technologies: an Italian national survey," Frontiers in Digital Health, vol. 8, p. 1718274, 2026.

[3] Z. Zhu, L. Liu, W. Zhang, C. Jiang, X. Wang, and J. Li, "Design and motion control of exoskeleton robot for paralyzed lower limb rehabilitation," Frontiers in Neuroscience, vol. 18, p. 1355052, 2024.

[4] L. Su et al., "Rear-Supported Lower-Limb Exoskeleton: Design Implementation and Experimental Validation of Assistive Performance," Annals of the New York Academy of Sciences, vol. 1556, no. 1, p. e70171, 2026.

[5] Y. Du, H. Wang, S. Qiu, W. Yao, P. Xie, and X. Chen, "An advanced adaptive control of lower limb rehabilitation robot," *Frontiers in Robotics and AI*, vol. 5, p. 116, 2018.

[6] Y. Tu, A. Zhu, J. Song, H. Shen, Z. Shen, X. Zhang, *et al.*, "An adaptive sliding mode variable admittance control method for lower limb rehabilitation exoskeleton robot," *Applied Sciences*, vol. 10, p. 2536, 2020.

[7] X. Gao, P. Zhang, X. Peng, J. Zhao, K. Liu, M. Miao, *et al.*, "Autonomous motion and control of lower limb exoskeleton rehabilitation robot," *Frontiers in Bioengineering and Biotechnology*, vol. 11, 2023.

[8] H. K. Khalil and L. Praly, "High-gain observers in nonlinear feedback control," *International Journal of Robust and Nonlinear Control*, vol. 24, pp. 993-1015, 2014.

[9] S. Li, J. Yang, W.-H. Chen, and X. Chen, *Disturbance observer-based control: methods and applications*: CRC press, 2014.

[10] A. Mohammadi, M. Tavakoli, H. J. Marquez, and F. Hashemzadeh, "Nonlinear disturbance observer design for robotic manipulators," *Control Engineering Practice,* vol. 21, pp. 253-267, 2013.